Three-dimensional coded aperture scintigraphy proposed for early tumor detection

K. Hussain[1,2*], M.I. Saripan[1], M.A. Alnafea[3], D. Mahboub[4], R. Mahmud[5], W.A. Wan Adnan[1], D. Xianling[6]

[1]*Department of Computer and Communication System Engineering, Universiti Putra Malaysia, Serdang, Malaysia*
[2]*Department of Computer Science, National University of Computer and Emerging Sciences, Islamabad, Chiniot-Faisalabad Campus, Chiniot 35400, Pakistan*
[3]*Physics Department, University of Hail, Ha'il 81451, Kingdom of Saudi Arabia*
[4]*Department of Radiological Sciences, College of Applied Medical Sciences, King Saud University, Riyadh 11433, Kingdom of Saudi Arabia*
[5]*Faculty of Medicine and Sciences, Universiti Putra Malaysia, Serdang, Malaysia*
[6]*Department of Biomedical Engineering, Chengde Medical University, Chengde City, Hebei, China*

► *Original article*

ABSTRACT

Background: Modified Uniformly Redundant Array (MURA) Coded Aperture (CA) is a type of mask recently proposed for breast tumor imaging. Such masks have been frequently used in nuclear medicine clinical applications for the past two decades. All CA imaging methods are still limited to planar imaging, with only a few exceptions where they can be used for thin 3D imaging. At present, there is no commercially available SPECT camera that employs CA technology. **Materials and Methods:** This paper is investigating the proof-of-concept of the MURA CA mask for 3D breast tumor imaging. Such image formation performed well in planar imaging, but it is not fully evaluated for thick sources in 3D imaging. This paper demonstrated the performance of MURA in 3D breast imaging. The proposed imaging system uses a MURA mask and antimask dual reconstruction, and the raw projections are reconstructed using an iterative algorithm, Maximum Likelihood Expectation Maximization (MLEM). **Results:** The MURA antimask-reconstructed images are summed with mask images to enhance sensitivity, and the resultant image with up to 3 mm lesion diameter can be detected. The reconstructed image quality is measured by plotting profiles and by measuring contrast-to-background ratio, peak-signal-to-noise ratio, and mean square error. **Conclusion:** The proposed scintigraphy system has successfully reconstructed a breast phantom with a lesion of 3 mm diameter and tumor-to-background ratio of 10:1 using a MURA CA mask. Therefore, MURA 3D scintigraphy can be used to diagnose cancer at an early stage.

INTRODUCTION

Cancer is a deadly illness that develops in a single organ or tissue and spreads uncontrollably. Breast cancer is a common malignancy among women throughout Europe, Australia, North America, Asia, United State and a number of Latin American nations [1, 2]. The last statistical update is from the American Cancer Society, indicating that it is the second largest cause of cancer mortality among women overall, after only lung cancer [3-6]. Early detection of breast cancer is an aim that would enable better outcomes and survival. X-ray Mammography has been used for more than five decades to investigate symptomatic and asymptomatic women of selected age groups. The breast tissues of the majority of screened women under the age of 50 have dense breasts, i.e., more glandular tissues. The lesions are obscured, which results in false negative mammography.

Scintigraphy imaging uses radiotracer such as ^{99m}Tc-sestamibi inside the patient's body unlike the mammography where external radiations are used for imaging. Conventionally, Scintigraphy imaging is achieved with the help of high-resolution parallel hole collimator [7]. This technique suffers from clinical limitations as it has less reliability in detecting small lesions (less than one centimeter in diameter) due to trade-off between sensitivity and resolution [8].

The coded aperture (CA) masks have been studied extensively for its application in medical imaging as an alternative to parallel-hole collimator. The attractive feature of CA image formation methods are the high sensitivity, contrast, and signal-to-noise ratio that has a significant impact on the quality of image under investigation [9]. The coded aperture imaging techniques were originally developed for X-ray astronomy in far-field geometry [10]. In 1972, Barrett used a Fresnel zone plate to visualize a nuclear

medicine thyroid phantom [11]. Fenimore introduced the idea of uniformly redundant array (URA's) coded aperture binary mask that has more attractive imaging properties [12]. The first viable form of CA binary mask was proposed by Mertz and Young [13]. A detailed overview of the coded aperture imaging was given by Accorsi [14], Starfiel [15], and Joshi [16]. Among the different patterns of CA, cyclic difference arrays like URA's, and modified uniformly redundant array (MURA) [17] have been investigated as the most promising patterns of coded aperture with strong transmission qualities (i.e., the region transparent to gamma particles and opaque is the same) and flat (have zero) side lobes.

This study proposed a CA based 3D scintigraphy which is a continuation of work by authors [18] addressing and suggesting an imaging system to be hopefully used for the early detection of breast cancers. Although, there is no one method that can be applied to breast cancer detection cases without showing certain clinical or technical limitations. This is a continuation of work by the authors by addressing and suggesting an imaging system to be hopefully used for the early detection of breast cancers. One of the method that has recently been applied is the use of mosaic MURA CA [18] coupled to a full field clinical gamma camera imaging system. This system produces a digitized 3D scintimammography image of an anthropomorphic female breast phantom [19] containing a (3 mm tumor) that has been obtained from a single projection. The computer program then searches for anomalous regions of density, mass, or calcification that may suggest the presence of cancer. The suggested approach highlights these spots on the images and, ideally, informs the radiologist to the need for additional study in the near future. The tissue composition of simulated compressed female breast phantom was taken from ICRU report 44 [20].

The main aim of this research is to use MURA CA mask antimask technique and simulated breast phantom with different sizes of tumors varying from 8 mm to 3 mm in diameter. This mask antimask method has successfully reconstructed breast phantom with a 3 mm lesion using tumor-to-background ratio (TBR) 10:1. The quality of reconstructed images is evaluated by plotting profiles through the center of the tumor for consecutive slices of 1 mm thinkness and also by measuring the PSNR [21], CBR [22], and MSE [21] of all the reconstructed images.

Several Monte Carlo Softwares can be used, including PENELOPE [23], MCNP [24], and GATE [25]. GATE was developed by OpenGate collaboration and is used in this paper.

MATERIALS AND METHODS

In this section, materials and methods used in this study are discussed. It consists of modeling geometrical design, coded aperture mask, breast phantom activity and the reconstruction method.

Geometrical design

The first step of this section describes the detail of experiment setup, including 3D anthropomorphic female breast phantom and coded aperture mask. The 3D anthropomorphic female breast phantom given in figure 1 is simulated using GATE according to the geometrical setup shown in figure 2. The coded aperture mask is built from MURA binary patterns of 173 × 173 elements. The detector and backscattering compartment were made of sodium iodide (NaI) and Pyrex, respectively, having dimensions of 69.2 × 69.2 cm² to match magnification factor, which is 4 in all experiments. The mask whole size is fixed at 1 mm throughout all the experiments. The coded mask and detector are shielded by tungsten material 1.5 mm thick to stop the false count that can blur the reconstructed images. The 1.5 mm thick tungsten can stop up to 99.4 % gamma radiation at the energy of 140 keV emitting from ^{99m}Tc, an excessively used radiopharmaceutical agent in nuclear medicine. At the center of compressed hemi-ellipsoidal phantom, given in figure 2, the magnification coefficient m is 4, where m is the ratio of mask projection on detector to actual size of the mask. Object magnification which is the ratio of the distance of the mask from the detector to the distance from the source object is 3.

The other important parameter is the field-of-view which is the range of source direction that can be modulated by the CA mask is calculated as 23.06 cm at the center of phantom. In near-field CA imaging, a geometric resolution is an important parameter, and it refers to the system's resolution. Therefore, the geometric design parameters must be modeled carefully. The reconstruction of breast slices is affected by the magnification factor which vary with respect to the depth of the phantom. The phantom depth is 40 mm, spanning up to 40 slices with 1 mm thickness. Therefore, for full reconstruction over all slices, the magnification factor varies over the range of 3.5 to 4.75, from the first slice at the distance of 80 mm to the last slice at the distance of 120 mm.
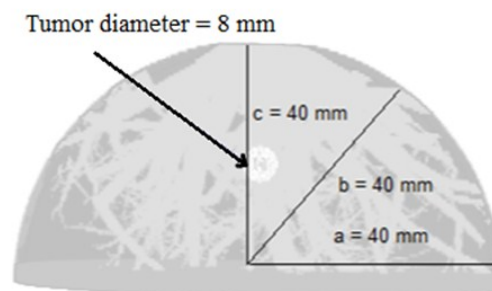

Figure 1. Illustration of compressed anthropomorphic breast phantom with a tumor of 8 mm diameter.
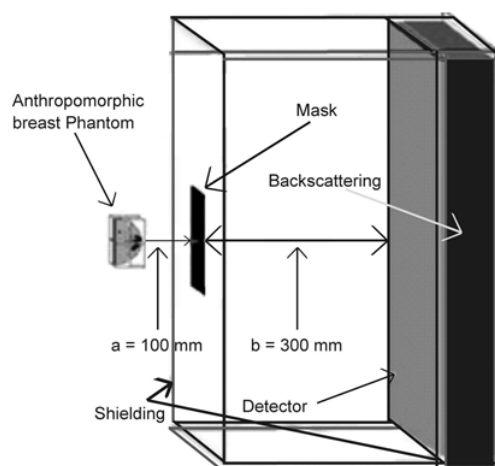
Figure 2. Design diagram of simulation setup using GATE

Phantom activity

The breast phantom simulated is hemi-ellipsoid in all experiments, but the lesion size is different in each experiment. In the case of breast examination, the examinee is often injected with a dose of 20 mCi of ^{99m}Tc-sestamibi into the vein of opposite arm of known breast abnormality and asked to wait for 5 to 10 minutes before screening. The total emission of gamma particles is nearly 750 million gamma particles in a 4pi solid angle. Although the emission of ^{99m}Tc from different parts of body may be different due to variations in blood flow, the ^{99m}Tc-sestamibi emissions from the tumor part of the breast are higher than from the rest of the breast, and this rate is in correlation with the size of the lesion. This paper used TBR 10:1, where tumor activity is taken as ten times more than breast activity.

Coded aperture mask

The CA imaging suffers from various noises, including decoding, background, and particle angle modulation, that affect the quality of the reconstructed image. Different CA mask has different performance and the one having delta-like correlation function is considered suitable for medical imaging. The MURA mask, given in figure 3, has a perfect delta correlation function which can be seen from figure 4 and thus it is considered an optimum choice for medical imaging.

GATE digitizer

The GATE, a Monte Carlo simulation tool, is used to simulate the phantom with the MURA coded aperture. The GATE includes a digitizer module that simulates the behavior of the scanning detectors and signal processing chain [26]. The digitizer contains a module 'single' that retains the particle's starting coordinates as well as its coordinates when it deposits energy into the scintillation crystal. The digitizer has components that allow the user to blur particle position and energy, as well as configure the energy window. Gaussian blurring is used to blur spatial and energy resolution to 1 mm and 10%,

respectively, smaller values than geometric resolution. The energy window for radiations with maximum energy of 140 keV emitting from ^{99m}Tc is 10% which is between 126 keV and 154 Kev.
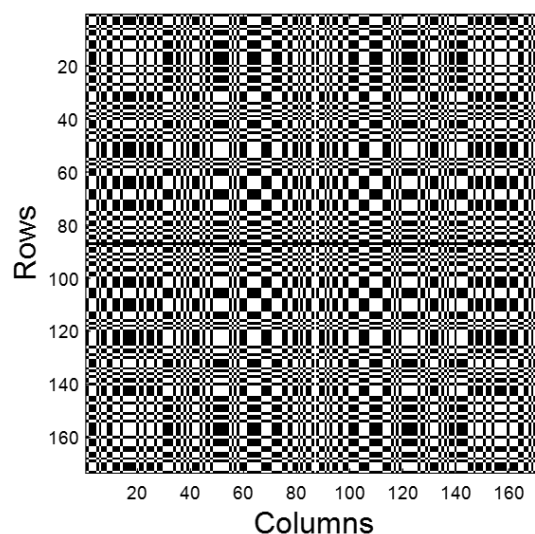

Figure 3. MURA CA mask binary pattern of 173 × 173 elements.
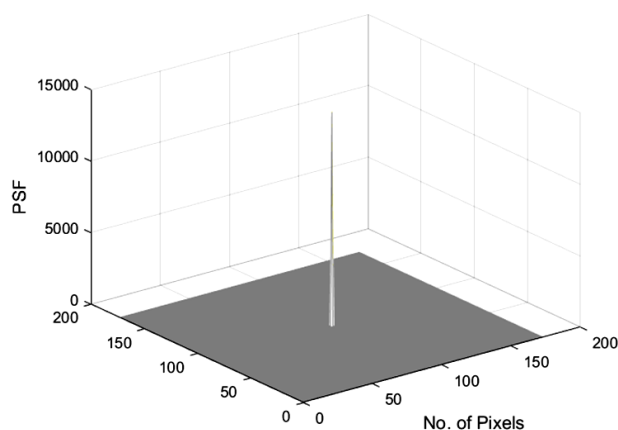

Figure 4. A 3D response function (PSF) of autocorrelation MURA CA mask.

Image reconstruction

In coded aperture, imaging is a two-step process, encoding and decoding/reconstruction [27]. For reconstruction, different methods are used, including correlation method, filtered back projection, and iterative method.

This paper follows the reconstruction method that was already used in our previous paper that employs MLEM iterative algorithms for 3D breast phantom reconstruction [22]. The MURA mask/antimask images are reconstructed using each slice 1 mm thick and stacked in order of reconstruction to generate the 3D image. Figure 5 represents the images reconstructed using MLEM with mask, antimask, and the summed image of both for tumor depth of 50 % to 75 % at slice level. The summed slices of mask and antimask are better than the individual one's and give a significantly improved 3D image when slices are stacked to generate the 3D reconstructed image of anthropomorphic female breast phantom.
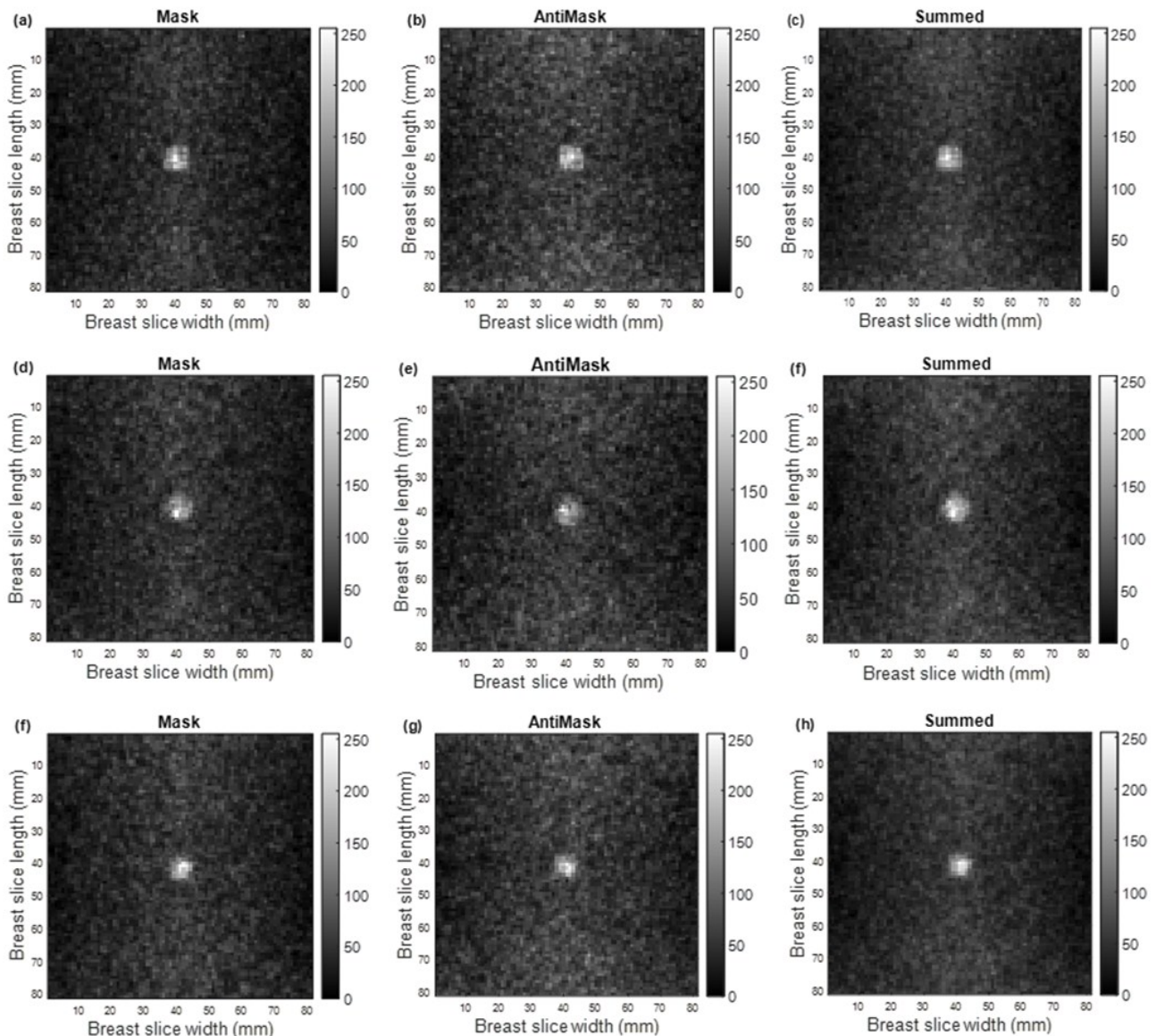
Figure 5. This figure illustrates the reconstructed slices of an 8 mm tumor with MURA mask/antimask are given as **(a)** mask at 50 % depth, **(b)** antimask at 50 % depth **(c)** summation of **(a)** and **(b)**, **(d)** mask at 62.5 % depth, **(e)** antimask at 62.5% depth, **(f)** summation of **(d)** and **(e)** slices, **(g)** mask at 75 % depth. **(h)** antimask at 75 % depth, **(i)** summation of **(g)** and **(h)** slices. The TBR used is 10:1.

RESULTS

In this section, results of experiments conducted using a MURA mask and an anthropomorphic breast phantom with varying tumor diameters from 8mm to 3mm were reported. The reconstructed images are evaluated by plotting profiles through the center of the tumors and by measuring PSNR, CBR, and MSE of the reconstructed images. All simulations are done with a breast activity of 20 mCi, which gives off 750 million photons over a ten-minute acquisition. The summed images of MURA mask/antimask generate an image with enhanced quality making it possible to visualize as small tumors as 3 mm in diameter. The MLEM iterative reconstruction performs well at slice-level reconstruction that is used in this paper, the 3D reconstructed images of MURA mask and antimask are given in figure 6. The 3D images of

mask and antimask of 8 mm have noise along the axial directions, but still, it is possible to detect the lesion size of 3 mm after summing both mask and antimask reconstructed image in 3D. Figure 7 part a, b, c and d represents the subtracted 3D images of mask anitmask while figure 7 part e, f, g and h shows the summed images of mask and antimask. The antimask is basically a rotated version of the mask by 90 degrees. The subtracted images lose the quality and become worse than the individual mask and antimask images, while the summed images have significantly improved, and it became easy to detect the tumor until 3 mm in size. The image quality is important to get the desired diagnosing consequences. The CBR, PSNR, and MSE measured from a planar form of the 3D tumor images can give a considerable idea about the quality of reconstructed images. Figure 8 explains the results of the image

quality measurements for summed images of all simulated lesions. Peak signal-to-noise ratio and contrast-to-background ratio are at their maximums for lesions that are 8 mm in diameter and decline as the lesion diameter increases. Additionally, the MSE increases as the lesion diameter decreases because the background non-uniformity increases as the lesion size decrease. Table 1 shows the values of reconstructed image quality in terms of different parameters, as given below.
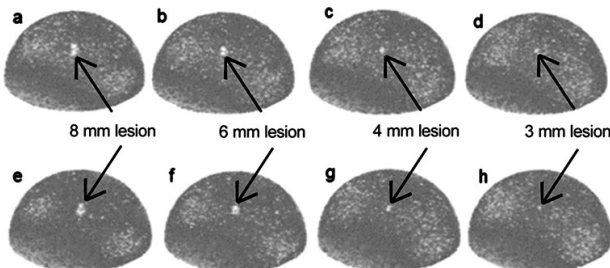

Figure 6. This figure illustrates MURA CA mask and antimask 3D reconstructed images of different lesion diameters. The mask antimask subtracted images are given in **(a)**, **(b)**, **(c)** and **(d)** for 8 mm, 6 mm, 4 mm and 3 mm while mask antimask summed images are given in **(e)**, **(f)**, **(g)** and **(h)**.
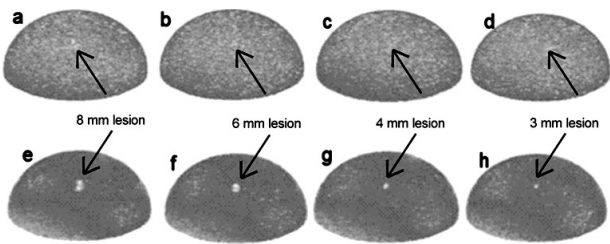

Figure 7. MURA CA mask and antimask 3D reconstructed images of different lesion diameters. The mask antimask subtracted images are given in **(a)**, **(b)**, **(c)** and **(d)** for 8 mm, 6 mm, 4 mm and 3 mm while mask antimask summed images are given in **(e)**, **(f)**, **(g)** and **(h)**.

Table 1. The PSNR, CBR, and MSE were assessed from reconstructed images of breast variable lesion diameters and a fixed TBR ratio of 10:1.

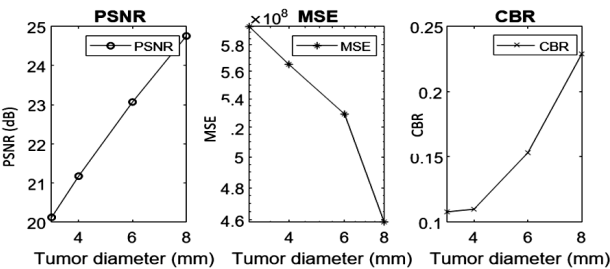| Diameter vs. Parameter	3 mm	4 mm	6 mm	8 mm
CBR	0.10771	0.109765	0.153163	0.22905
PSNR	20.11602	21.17158	23.07028	24.76181
MSE	5.94E+08	5.65E+08	5.29E+08	4.59E+08

Figure 8. Results of peak signal-to-noise ratio **(a)**, contrast-to-background ratio **(b)**, and mean square **(c)** for breast phantom images obtained from summed MURA mask/antimask and reconstructed using MLEM.

The graphical presentation of image performance parameters of the 3D breast phantom reconstruction is presented in figure 8. Peak signal-to-noise ratio and contrast-to-background ratio values are greater for larger tumors and decrease gradually as tumor diameter shrinks. In addition, the mean square error is minimal for an 8 mm tumor and grows as the tumor size decreases. All graphs are correlated with the diameter of the tumor and present enough statistics to visualize the 3 mm tumor in a three-dimensional view.

Figure 9 represents the correlation of tumor profiles taken from central slice S1 and adjacent to central slice S2 with 1 mm thickness. Profiles of slices S1 and S2 have clear peaks at the center and a strong correlation between themselves. The profile of 3 mm lesion diameter has also peaks at center and both peaks of S1 and S2 slices have a correlation at the center only that agree to depict the presence of lesion. Other peaks outside the center in 3 mm lesion have no correlation. Therefore, it can be concluded that using the method discussed in this paper, up to 3 mm diameter lesion can be detected to treat cancer at an early stage that can potentially save the patient's life.
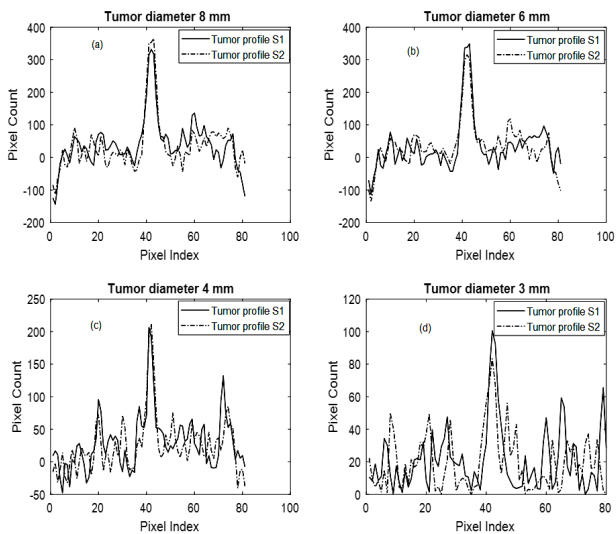

Figure 9. This figure illustrates the breast phantom vertical profile through the center of the tumor using MURA mask/antimask with a diameter of 8 mm **(a)** and 6 mm **(b)**, 4 mm **(c)**, and 3 mm **(d)**. TBR is 10:1.

DISCUSSION

Scintigraphy imaging modality is used in many hospitals and it has the ability to provide planar and 3D imaging of radionuclide distribution with recognized applications in imaging the breast, heart, liver, brain, and bones [32]. The majority of the clinical gamma cameras have a spatial resolution of around 10 mm [33]. The dedicated breast imaging camera, BSGI (DILON 6800 Gamma Camera), also has the ability to detect breast lesions around 10 mm for

dense breast [34]. Hruskaa *et al.* discussed the different papers that addressed the breast cancer for lesion around 10 mm [35]. Dong *et al.* [36] investigated the breast tumor using 3D imaging with different TBR and lesion sizes and remained successful in detecting lesion of 10 mm with TBR 10:1. The parallel -hole collimator technique suffers from clinical limitations as it has less reliability in detecting small lesions (less than one centimeter in diameter) due to trade-off between sensitivity and resolution. An alternative coded aperture based tomographic imaging approach was proposed by Cannon *et al.* [37].

Coded aperture-based imaging is continuously evolving in nuclear medicine, and a lot of work is reported on coded aperture imaging [9,38,39]. Jeong *et al.* [40] used planar gamma camera image reconstruction using a coded-aperture mask to overcome the artifacts of reconstruction in conventional reconstruction. MediPROBE, a planer-coded aperture imaging system's performance was assessed by Russoa *et al.* [41]. Moreover, Schwarz *et al.* [42] suggested an imaging system based on movable pinhole arrays, but it was for imaging small planar objects. Christopher *et al.* presented results of CA for point source and distributed sources [43]. Zhiping *et al.* has done significant work on planar coded-aperture imaging and 3D rat heart imaging, a small animal with limited performance [29]. Accorsi [14], and David [15] have discussed coded aperture imaging using 2D thyroid phantom and a 2D Shepp-Logan respectively but their study was based on planar CA imaging. Alnafea investigated planar breast imaging with coded aperture for varying TBR and lesion sizes [44]. Olga *et al.* has successfully detected 5 mm ×5 mm ×5 mm tumor using uniformly redundant array CA planar imaging [45]. Kadri *et al.* has also investigated the planar breast imaging using different sizes and were successful in detecting 8 mm and 5 mm lesion [46]. However, there is still no 3D breast imaging system using coded aperture technology.

To simulate scintigraphy, 3D compressed realistic an anthropomorphic female breast phantom has been developed and simulated using GATE. This study examines a moderately compressed breast phantom in a cranio-caudal-projection i.e., a similar view to that used in conventional X-ray mammography. The performance of such an imaging system is modelled by the GATE and images are reconstructed by MLEM. This imaging system was quantitatively evaluated using variable parameters: the detected photon from tumor, spatial resolution, photon statistics and lesion visibility of the system at tumor-background activity ratio of 10:1.

The proposed method has successfully presented sufficient statistics to detect as small a lesion as 3 mm, placed in the center of the 3D anthropomorphic breast phantom. The image profiles through the center of the tumor have a clear identification of the lesion inside the breast center that is detectable with the given setup of coded aperture imaging system. The image quality measured shows enough contrast-to-background ratio that the tumor is visible and can easily be diagnosed from summed images of MURA mask antimask using MLEM dual reconstruction. The coded aperture has been studied extensively for its application in medical diagnosis, but it's still limited to planar imaging or thin 3D imaging. No coded aperture-based imaging was discussed previously for 3D breast imaging. The radiation contribution from heart, chest, and lungs is not included in this study. The patient is housed in a lead chamber to shield the radiations other than breast.

CONCLUSION

The MURA CA mas/antimask performs remarkably well when combined with MLEM reconstruction. This study has presented proof of concepts that 3D reconstruction of the breast phantom for early breast cancer detection up to a 3 mm lesion is possible using MURA CA mask antimask with MLEM reconstruction. The reconstructed images of MURA mask and antimask are subtracted as well as summed. The subtracted images lost sensitivity and worsened the resultant images, making it difficult to visualize the lesion from subtracted images, while the summed images increased the sensitivity and increased the statistics, and thus a 3 mm lesion can be easily detected. Therefore, it can be concluded that the detection of a 3 mm lesion in 3D anthropomorphic breast imaging is possible with TBR 10:1. As a result of its improved efficacy, its implementation can be extended to other organs to identify a wide variety of cancerous cells, including heart, liver, and lung. In the future, artificial intelligence-based reconstruction techniques can be used for image formation purposes which may further improve the quality of reconstructed images.

REFERENCES

1. Giaquinto AN, Sung H, Miller KD, *et al.* (2022) Breast cancer statistics. *Cancer J Clin,* **72***(6): 524-541.*

2. Yaffe MJ and Mainprize JG (2011) Risk of radiation-induced breast cancer from mammographic screening. *Radiology,* **258***(1): 98-105.*

3. Giaquinto AN, Miller KD, Tossas KY, *et al.* (2022) Cancer statistics for African American/Black People. *CA Cancer J Clin,* **72***(3): 202-29.*

4. Miller KD, Ortiz AP, Pinheiro PS, *et al.* (2021) Cancer statistics for the US Hispanic/Latino population 2021. *CA Cancer J Clin,* **71***(6): 466-87.*

5. Islami F, Goding Sauer A, Miller KD, *et al.* (2018) Proportion and number of cancer cases and deaths attributable to potentially modifiable risk factors in the United States. *CA Cancer J Clin,* **68***(1): 31-54.*

6. Gallicchio L, Devasia TP, Tonorezos E, *et al.* (2022) Estimation of the number of Individuals living with metastatic cancer in the United States. *JNCI J Natl Cancer Institute,* **114***(11): 1476-1483.*

7. Pato LRV, Vandenberghe S, Zedda T, Van Holen R (2015) Parallel-hole collimator concept for stationary SPECT imaging. *Phys Med Biol, [Internet].* **60***(22): 8791-807.*

8. Holen R Van, Vandenberghe S, Staelens S, Lemahieu I (2008) Comparison of 3D SPECT imaging with a rotating slat collimator and a parallel hole collimator. *IEEE Nucl Sci Symp Conf Rec, 2008; (mm):4592-7.*

9. Schellingerhout D, Accorsi R, Mahmood U, *et al.* (2002) Coded aperture nuclear scintigraphy: A novel small animal imaging technique. *Mol Imaging,* **1***(4): 344–53.*

10. Proctor RJ, Skinner GK, Willmore AP (1979) The design of optimum coded mask X-ray telescopes. *Oxford Acadamic J,* **187***(3): 633-643.*

11. Barrett HH (1972) Fresnel Zone Plate Imaging in Nuclear Medicine. *J Nucl Med,* **24***(1): 2014–5.*

12. Fenimore EE and Cannon TM (1978) Coded aperture imaging with uniformly redundant arrays. *Appl Opt,* **17***(3): 337-47.*

13. Mertz L and Young NO (1996) Fresnel Transformations of Images. 1996. *SPIE milestone series ms,* **128**, 44-49.

14. Accorsi R (2001) Design of near-field coded aperture cameras for high-resolution medical and industrial gamma-ray imaging. PhD Thesis, *Massachusetts Inst Technol. 2001; 2001; Massachusetts, USA.*

15. Starfiel DM (2009) Towards clinically useful coded apertures for planar nuclear medicine imaging. *Phys Med Biol [Internet].* **36***(4): 125-33.*

16. Joshi S (2014) Coded aperture imaging applied to pixelated CdZnTe detectors. Dissertations and Theses (Ph.D. and Master's). *University of Michigan, Ann Arbor, USA.*

17. Fenimore EE and Scientific LA (1978) Coded aperture imaging: predicted performance of uniformly redundant arrays. *Appl Opt,* **17***(22): 3562.*

18. Hussain K, Alnafea MA, Saripan MI, *et al.* (2022) An innovative concept of a 3D-coded aperture imaging system proposed for early breast cancer detection. *Diagnostics,* **12***(10): 2529.*

19. Bliznakova K, Bliznakov Z, Bravou V, et al. (2003) A three-dimensional breast software phantom for mammography simulation. *Phys Med Biol,* **48***(22): 3699-719.*

20. Goldstone K (1989) Tissue substitutes in radiation dosimetry and measurement, in: ICRU report 44. International Commission on Radiation Units and Measurements. WB Saunders; *1989, USA.*

21. Park S, Boo J, Hammig M, Jeong M (2021) Impact of aperture-thickness on the real-time imaging characteristics of coded-aperture gamma cameras. *Nucl Eng Technol,* **53***(4): 1266-76.*

22. Saad WHMM, Roslan RE, Mahdi MA, *et al.* (2011) Saripan MI. Monte Carlo design of optimal wire mesh collimator for breast tumor imaging process. *Nucl Instruments Methods Phys Res Sect A Accel Spectrometers, Detect Assoc Equip,* **648***(1):254-60.*

23. Baró J, Sempau J, Fernández-Varea JM, Salvat F (1995) PENELOPE: An algorithm for Monte Carlo simulation of the penetration and energy loss of electrons and positrons in matter. *Nucl Inst Methods Phys Res B,* **100***(1): 31–46.*

24. Briesmeister JF (2000) MCNPTM – A General Monte Carlo N-Particle Transport Code. *Los Alamos Natl Lab,* **2000***: 790.*

25. Jan S, Benoit D, Becheva E, *et al.* (2004) GATE : a simulation toolkit for PET and SPECT. *Phys Med Biol,* **49***: 4543–4561.*

26. Welcome to GATE's Documentation [Internet]. [cited 2022 Aug 14]. Available from: https://opengate.readthedocs.io/en/latest/index.html

27. Nudelman s, D.D P, Simpson RG, Barrett HH (1980) Imaging for medicine ultrasonics and thermography. *Plenum Press, New York. 1980. 217-311.*

28. Mu Z and Liu Y-HH (2006) Aperture collimation correction and maximum-likelihood image reconstruction for near-field coded aperture imaging of single photon emission computerized tomography. *IEEE Trans Med Imaging,* **25***(6): 701-11.*

29. Mu Z, Dobrucki LW, Liu YH (2016) SPECT imaging of 2-D and 3-D distributed sources with near-field coded aperture collimation: Computer simulation and real data validation. *J Med Biol Eng,* **36***(1): 32-43.*

30. Martineau A, Rocchisani JM, Moretti JL (2010) Coded aperture optimization using Monte Carlo simulations. Nucl instruments methods phys res sect a accel spectrometers. *Detect Assoc Equip,* **616***(1): 75-80.*

31. Zhang R, Tang X, Gong P, *et al.* (2020) Low-noise reconstruction method for coded-aperture gamma camera based on multi-layer perceptron. *Nucl Eng Technol,* **52***(10): 2250-61.*

32. Gao S, Jia B, Feng G, *et al.* (2020) First-in-human pilot study of an integrin α6-targeted radiotracer for SPECT imaging of breast cancer. *Signal Transduct Target Ther,* **5***(1): 2-4.*

33. SPECT imaging applications to myocardial perfusion and brain imaging. Available from: https://openmedscience.com/spect-imaging/

34. Liu H, Zhan H, Sun D, Zhang Y (2020) Comparison of BSGI, MRI, mammography, and ultrasound for the diagnosis of breast lesions and their correlations with specific molecular subtypes in Chinese women. *BMC Med Imaging,* **20***(1): 1-10.*

35. Hruska CB and O'Connor MK (2013) Nuclear imaging of the breast: Translating achievements in instrumentation into clinical use. *Med Phys,* **40***(5): 1-23.*

36. Dong X, Saripan MI, Mahmud R, *et al.* (2017) Determination of the optimum filter for 99mTc SPECT breast imaging using a wire mesh collimator. *Pakistan J Nucl Med,* **7***(1): 9-15.*

37. Cannon TM and Fenimore EE (1979) Tomographical imaging using uniformly redundant arrays. *Appl Opt,* **18***(7): 1052.*

38. Odinaka I, O Sullivan JA, Politte DG, *et al.* (2017) Joint system and algorithm design for computationally efficient fan beam coded aperture X-ray coherent scatter imaging. *IEEE Trans Comput Imaging,* **3***(4): 506-21.*

39. Meikle SR, Fulton RR, Eberl S, *et al.* (2001) An investigation of coded aperture imaging for small animal SPECT. *IEEE Trans Nucl Sci,* **48***(3): 816-21.*

40. Jeong M and Kim G (2021) MCNP-polimi simulation for the compressed-sensing based reconstruction in a coded-aperture imaging CAI extended to partially-coded field-of-view. *Nucl Eng Technol,* **53***(1): 199-207.*

41. Russo P, Di Lillo F, Corvino V, *et al.* (2019) CdTe compact gamma camera for coded aperture imaging in radioguided surgery. *Phys Medica,* **69***(2019): 223-32.*

42. Schwarz A, Shemer A, Danan Y, *et al.* (2020) Gamma radiation imaging system via variable and time-multiplexed pinhole arrays. *Sensors (Switzerland),* **20***(11): 1-14.*

43. Wahl CG, Brown S, Kaye W, *et al.* (2018) Coded - Aperture Imaging with High - Resolution Large - Volume CZT. *2018 IEEE Nucl Sci Symp Med Imaging Conf Proc, C: 1-5.*

44. Alnafea M (2007) Coded aperture breast tumour imaging using a full-size clinical gamma camera. PhD Thesis, Univ Surrey, UK.

45. Vassilieva OI and Chaney RC (2002) Method for reducing background artifacts from images in single-photon emission computed tomography with a uniformly redundant array coded aperture. *Appl Opt,* **41***(7): 1454.*

46. Kadri O and Alfuraih A (2019) Monte Carlo assessment of coded aperture tool for breast imaging: a Mura-mask case study. *Nucl Sci Tech,* **30***(11): p.164.*